CMLS, Cell. Mol. Life Sci. 61 (2004) 951–960
1420-682X/04/080951-10
DOI 10.1007/s00018-003-3455-3

CMLS Cellular and Molecular Life Sciences

Research Article

Helix H1 of the prion protein is rather stable against environmental perturbations: molecular dynamics of mutation and deletion variants of PrP(90–231)

S. Santini[a] **and P. Derreumaux**[b,*]

[a] Information Génomique et Structurale, UPR 2589 CNRS, 31 Chemin Joseph Aiguier, 13402 Marseille Cedex 20 (France)
[b] Laboratoire de Biochimie Théorique, UPR 9080 CNRS, Institut de Biologie Physico-Chimique, 13 rue Pierre et Marie Curie, 75005 Paris (France), Fax: + 33 1 58 41 50 26, e-mail: Philippe.Derreumaux@ibpc.fr

Received 16 December 2003; received after revision 16 January 2004; accepted 21 January 2004

Abstract. We need to understand the underlying factors that promote or reverse the amyloid-type structure of the prion protein (PrP). In an earlier study, we showed that mutations within the first β strand can extend the short β sheet in the normal protein into a larger sheet at neutral pH. To determine the impact of the point mutation P102L and the deletion of either the first or the second β strand on PrP, we performed further long molecular explicit water dynamics simulations. The trajectories show that all mutations do not exert a uniform effect on the dynamics of the N-terminal tail. The results of the deletion of the two β strands confirm the idea that partially unfolded conformations are involved in the structural transition. In the deletion variants, the α helices H2 and H3 are disordered, while helix H1 is either fully stable or partially disordered. This finding, consistent with recent spectroscopic analyses on peptides spanning helix H1 and flanking sequences, demonstrates that unfolding of the full domain containing helix H1 is not an early step in PrP interconversion. This result also raises questions regarding a current view of PrP^{Sc} structure that transforms helix H1 into a β sheet conformation.

Key words. Molecular dynamics simulation; mutation; prion; deletion; protein structure; unfolding.

Transmissible spongiform encephalopathies (TSEs) are fatal neurodegenerative diseases and include Creutzfeldt-Jakob disease, Gerstmann-Straussler-Scheinker syndrome and fatal familial insomnia in humans, scrapie in sheep, and bovine spongiform encephalopathy. The 'protein-only' hypothesis states that TSEs are devoid of informational nucleic acid and result from the conversion of a monomeric soluble cellular protease-sensitive prion protein (PrP^{C}) into a multimeric insoluble protease-resistant PrP^{Sc} [1]. Mammalian PrP^{C} is a highly conserved secretory cell surface glycoprotein of approximately 210 amino acids (residues 23–231) that contains two glycosylation sites at Asn181 and Asn197, a glycosyl-phosphatidyl-inositol anchor at its C-terminal residue 231 and a single disulfide bond between Cys179 and Cys214. The three-dimensional nuclear magnetic resonance (NMR) structure of recombinant PrP spanning residues 90–231 (referred to as PrP90–231) from Syrian hamster [2] consists of a disordered tail (residues 90–123) and a globular domain with three α helices (H1: residues 145–153; H2: 172–194; H3: 200–225) and a short antiparallel β sheet (strand S1: residues 129–132; strand S2: 160–163). Although the NMR structures from mouse [3], cattle, human [4] and Syrian hamster are very similar, conformational changes are observed within the loops connecting the helices and even in the length of the

* Corresponding author.

helices. Recently, the crystal structure of a dimeric form of recombinant human PrP was reported, the dimer being formed by swapping of helix H3 and an intermolecular disulfide bridge [5]. In contrast to PrP^{C} which has a low β sheet content (3–8%), PrP^{Sc} has 40% β sheet [6] but no high-resolution structure is yet available [7, 8].

Despite intensive research, the molecular mechanism underlying the conformational conversion remains enigmatic. TSEs may arise sporadically, may be acquired by transmission of an infectious agent and may be inherited (familial forms) through more than twenty mutations in the human PrP gene [9, 10]. Most mutations are located in the structured core 124–226: strand S1 (M129V, G131V), helix H2 (D178N, V180I, T183A, H187R, T188A or T188K or T188R), loop between H2 and H3 (E196K, F198S) and helix H3 (E200K, D202N, V203I, R208H, V210I, E211Q, Q212P and Q217R). But, three mutations also occur within the disordered N-terminal tail: P102L, P105L and A117V. Mutations in the PrP gene are generally believed to promote the conformational conversion by destabilizing the native structure of PrP^{C} [11]. Although this has been confirmed for T183A, F198S and Q217R mutants [12, 13], it is not a general mechanism underlying the formation of PrP^{Sc} [14]. In an earlier molecular dynamics (MD) study, we showed that the mutations M129V and G131V within the first β strand can extend the short β sheet in the normal protein into a larger sheet at neutral pH [15]. This study complements previous MD simulations on A117V [16], D178N [17], T183A, V180I and Q217R variants [18]. This result, however, raises the question whether the mutations within the tail exert the same effect. As a first step, we decided to examine the mutation P102L. This mutation, which changes TSE incubation times [19], is also of interest because its impact on the thermodynamic stability of PrP is not fully understood. Cappai et al. [20] showed that mouse PrP23–231(P101L) – codon 101 in mouse but codon 102 in human – is associated with a significant decrease in α helix content, while Swietnicki et al. [21] reported that human PrP90–231(P102L) does not lead to any identifiable effects on secondary structure or stability. Because the P102L mutation can be coupled with codon 129 [22], we also examined the effect of the double mutation P102L-M129V. To this end, we performed MD simulations of wild-type PrP90–231 and its P102L and P102L-M129V variants for 4–8 ns at 320 K.

There is interest in approaches aimed at preventing or even reversing PrP^{Sc} formation. Soto et al. [23] partly reversed in vitro PrP^{Sc} to PrP^{C} using β sheet breaker peptides spanning PrP115–122 [23]. Caughey et al. [24] inhibited the conversion reaction in vitro using diferoylmethane. Another strategy involves the use of deletion variants. Eberl and Glockshuber [25] generated PrP121–231-H1 where helix H1 is deleted and replaced by the dipeptide Asn-Gly in order to facilitate a β turn between the strands. They showed that this variant, which partially retains α-helical structure, is strongly destabilized compared to wild-type PrP121–231. Vorberg et al. [26] extended this approach further: they showed that deletion of either the first or the second β strand significantly reduces the ability of PrP^{C} to be converted to PrP^{Sc} in a cell-free assay system. The conversion efficiency of both PrP deletion variants was found to decrease by ~75%. Based on the atomic contacts within the PrP^{C} structure, they proposed that deletion of strand S2 (referred to as PrP-S2) should destabilize PrP^{C} and lead to a misfolded protein, while deletion of strand S1 (PrP-S1) should not destabilize the protein, but rather modify the interactions between PrP^{C} and PrP^{Sc}. To test their hypotheses, we performed MD simulations of wild-type PrP and its PrP-S1 and PrP-S2 variants at 320 K for 4 ns and 298 K for 20 ns.

Materials and methods

Molecular modeling

All simulations were performed at neutral pH using the program GROMACS2.0 and the all-hydrogen energy function GROMOS96 [27]. As in our earlier study, the starting point was the NMR structure of Syrian hamster PrP90-231 [Protein Data Bank (PBB) entry 2PRP] [28]. The PDB entry 2PRP was chosen rather than the most recent entry 1B10 because 1B10 lacks the atomic positions of the 90–123 tail. Although the tail is presumably too disordered in 2PRP, as suggested by the experimentalists, its NMR-derived position is a better starting point than (i) any structural candidates suggested by fold recognition methods using the PrP90–124 sequence as a query and (ii) any conformations generated by ab initio molecular-modeling methods. The initial structures for P102L, P102L-M129V, PrP-S1 (residues 129–132 removed) and PrP-S2 (residues 160–163 removed) were constructed using the SWISS-MODEL server [29] and the resulting structures minimized using the EEF1 energy model [30]. EEF1 combines the CHARMM19 polar hydrogen potential energy function and a simple Gaussian model for the solvation free energy. We believe that the local minima generated by this procedure for the deletion variants have little impact on the dynamics at a 20-ns timescale.

All PrP models were then solvated in a cubic box of 70-Å sides with ~10,000 simple point charge (SPC) water molecules and simulated using periodic boundary conditions. Van der Waals interactions were truncated at 8.5 Å. The electrostatic treatment (12-Å truncation) is standard and allows a good trade-off between accuracy and computer time [17]. Note that a 10-Å truncation has also been used elsewhere [31]. The PrP models were minimized by 300 steps of steepest descent and 600 steps of conjugate gradient and then equilibrated at the desired

temperature for 50 ps under Cα atom restraints followed by 50 ps free of any atomic restraints. At this stage, MD simulations were performed in the canonical NPT (number of particles-pressure-temperature) ensemble. The time step for dynamics was 2.0 fs using the LINCS algorithm and the list of nonbonded interactions was updated every 20 fs. Temperature was controlled using a weak coupling to a bath of constant T (coupling time of 0.1 ps) and pressure by a weak coupling to a bath of constant P (1 atm, coupling time of 0.5 ps). All PrP models were simulated at 320 K for 4 ns. The temperature was set to 320 K to accelerate conformational sampling, but this T still favors the native state (T_m ~340 K [32]). The P102L variant was also simulated starting from the same structure using different initial velocities (runs R1 and R2) to check that different simulations on the same sequence produce equivalent results. The P102L-M129V variant was also simulated for 8 ns to determine the effect of extending the timescale on the calculated dynamics properties. Finally, wild-type PrP and its PrP-S1 and PrP-S2 deletion variants were subjected to MD simulations at 298 K for 20 ns. All runs covering 88 ns in total took 6 months on a cluster of 7 PII 500 MHz processors.

The trajectories were analyzed using several order parameters. These include (i) Cα root mean square (RMS) deviations of the residues 90–231, 124–226 or 128–214 from the MD average NMR structure (the trajectory from 100 to 200 ps was used to generate this structure; we emphasize that one single NMR conformer is available in the PDB entry 2PRP); (ii) Cα RMS fluctuations (RMSFs) relative to the average MD structure; (iii) percentage of secondary structure content using the DSSP program [33]; (iv) cluster analysis of the conformations and (v) fraction of native contacts. Following Day et al. [34], a contact is defined when aliphatic carbon atoms of two nonsequential side chains come within 5.4 Å or any other atom of two nonsequential side chains lies within 4.6 Å. Solvent-accessible surface areas were calculated using the GETAREA server [35]. The pictures were produced with MOLMOL software [36].

Validity of simulations

The validity of the present conclusions depends on several factors. The impact of force field and pH conditions on PrP dynamics has been discussed elsewhere [16, 31]. Here, we focus on two other points. First, the Syrian hamster sequence has been used for both the studies, while the P102L mutation occurs in humans, and the deletion mutants have been studied in mice neuroblastoma cells. The mouse and human PrP90–231 sequences share 94% and 89% identities, respectively, with hamster PrP90–231. The species variation has been studied in detail by MD simulations on hamster, human and bovine forms of the prion protein at neutral and low pH [37]. The results show that the dynamics of the protein core and the tail are essentially independent of the species. This suggests that our MD average properties using Syrian hamster can be extrapolated to human and mouse.

Second, we draw conclusions on the prion protein conformations extrapolating from nanosecond timescales. Clearly, the timescale accessible by the present explicit water simulations (20 ns at 298 K and 8 ns at 320 K) is several orders of magnitude smaller than the experimental folding time of PrP (0.2 ms at 278 K [38]). The millisecond timescale, however, is still beyond computer facilities using all-atom models [39]. As a result, we cannot exclude the possibility that the most populated structures of the deletion and mutation PrP variants may only capture the initial unfolding steps, and thus the present dynamic behavior has only qualitative significance.

Results and discussion

Wild-type and P102L PrPs have comparable overall dynamics

To determine whether the point mutation P102L induces structural changes in PrP^C, we performed 4-ns MD simulations of wild-type PrP, P102L (run 1), P102L (run 2) and P102L-M129V at 320 K. The minimized structures of P102L and P102L-M129V variants deviate by 0.4 Å from that of wild-type PrP.

Figure 1 shows the Cα RMS deviations of the residues 90–231 (fig. 1A) and 124–226 (fig. 1B) from the MD average NMR structure for all PrP models. The RMS deviations of residues 90–231 versus time fluctuate around 4.5 Å for wild-type PrP, 3.5 Å and 6.5 Å for P102L in runs 1 and 2, respectively, and 5.5 Å for P102L-M129V between 2 and 4 ns. Clearly, extending the PrP102L-M129V simulation from 4 to 8 ns does not change the results (see also table 1). The increased flexibility in P102L-M129V and P102L (run 2) with respect to wild-type PrP does not result from the structured core 124–226, but rather from the tail. The plots of Cα RMS deviations (fig. 1B) and Cα RMS fluctuations with respect to the average MD structures (fig. 1C) are highly superposable in the region 124–226. The largest differences in RMS fluctuations between all PrP models and for example between runs 1 and 2 of PrP102L variants are found in the loop between S1 and H1 (residues 134–142), the loop between S2 and H2 (residues 165–179) and the loop between H2 and H3 (residues 195–199). These three regions have been characterized by NMR to have low hydrogen-deuterium exchange protection factors in wild-type PrP [40].

The standard deviation of MD-generated secondary-structure percentage within the region 124–226 in table 1 is independent of the PrP model studied (α helix: 3.9% for wild-type PrP, 3.2% for P102L, 5.9% for P102L-M129V; β strand: 2.0% for wild-type PrP, 3.4% for

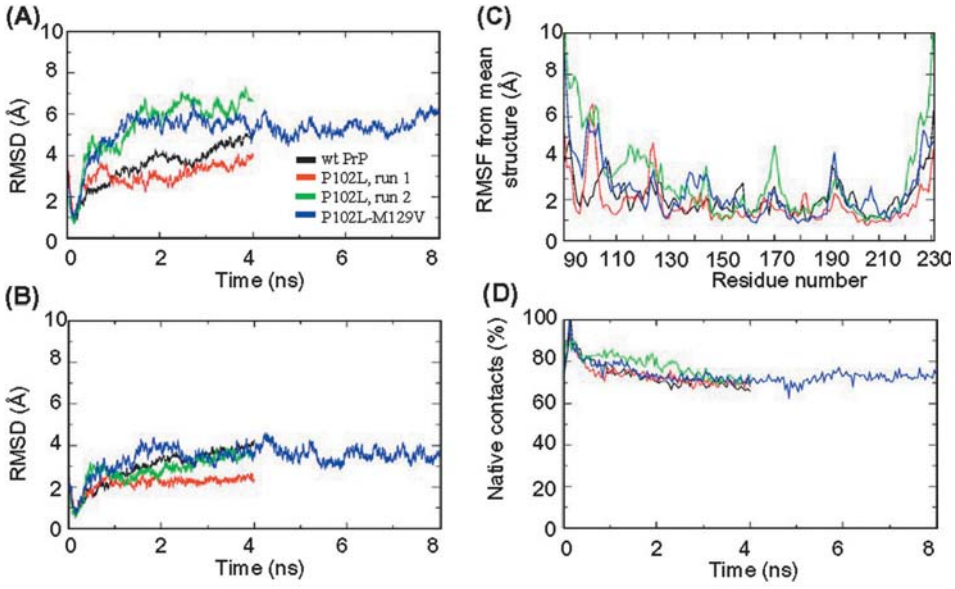

Figure 1. (*A–D*) Simulations of wild-type PrP90-231 and its P102L and P102L-M129V variants at 320 K. RMS deviations from the MD average NMR structure of the residues 90–231 (*A*) and residues 124–226 (*B*) as a function of time. RMSF from mean structure (*C*). Percentage of native contacts as a function of time (*D*). Red, P102L run 1; green, P102L run 2; blue, P102L-M129V; black, wild-type (wt) PrP.

Table 1. Secondary structures of the PrP90-231 models from MD simulations at pH 7.

PrP model	T (K)	ns	S_a	H_a	S_c	H_c	H1	H2	H3
wt	320	4	5.2 ± 2.3	37.3 ± 3.0	3.9 ± 2.0	51 ± 3.9	80	76	90
P102L (R1)	320	4	7.5 ± 2.0	41.6 ± 1.5	7.9 ± 2.5	57 ± 2.1	98	93	96
P102L (R2)	320	4	5.7 ± 4.2	38.7 ± 2.1	6.1 ± 4.2	53 ± 4.2	90	88	92
P102L–M129V	320	4	7.0 ± 2.6	33.6 ± 4.3	8.2 ± 3.0	46 ± 5.9	93	81	68
P102L–M129V	320	8	8.1 ± 2.9	32.7 ± 4.0	8.8 ± 2.9	45 ± 5.4	90	75	68
wt-S1	320	4	0.0	39.2 ± 2.9	0.0	55 ± 4.0	99	85	74
wt-S2	320	4	6.5 ± 2.3	28.1 ± 3.3	4.8 ± 2.1	42 ± 4.5	70	64	83
wt	298	20	7.5 ± 2.5	41.7 ± 2.1	7.8 ± 2.6	57 ± 2.8	99	91	97
wt-S1	298	20	0.0	34.1 ± 4.1	0.0	47 ± 5.6	91	80	67
wt-S2	298	20	1.7 ± 2.3	24.4 ± 6.4	1.1 ± 1.9	34 ± 8.7	64	42	65

The mean (M) and standard deviation (SD) of α helix (H) and β strand (S) percentages within residues 90–231 (subscript a) and residues 124–226 (subscript c) are expressed in the form M ± SD. The mean percentage of helices H1, H2 and H3 during the simulations are shown to the right. H1, H2 and H3 span residues 145–153, 172–194 and 200–225 in the NMR structure of wild-type (wt) Syrian hamster PrP90–231 [2]. For P102L, runs R1 and R2 use different random seeds. The second P102L–M129 simulation extends the previous one from 4 to 8 ns.

P102L, 3.0% for P102L-M129V). The MD average percentage of the α helix varies: 51% for wild-type PrP, 55% for P102L and 45% for P102L-M129V. This is in agreement with the NMR-derived percentages of human PrP mutants (48% for S170N and 58% for E200K [5]) and the MD-generated percentages on G131V (49%) and M129V (51%) [15]. We find that helix H1 is very stable in all simulations and that helix H3 is very dynamic in P102L-M129V: H3 is formed 68% of the time (on average broken into two parts, 200–204 and 209–220) versus 94% in P102L and 90% in wild-type PrP. This flexibility is, however, not surprising since helix H3 is shorter in mouse PrP, spanning residues 200–222 [3]. We also observe that the end terminal of helix H2 is very flexible in wild-type PrP and P102L-M129V (residues 190–194 are disordered), while it is very rigid in P102L. Such flexibility of the C-terminal portion of helix H2 has already been discussed [41]. In line with MD analysis of the G131V and M129V variants [15], the MD average percentage of β strand within the region 124–226 increases upon mutation: 3.9% for wild-type PrP, 6.1% for P102L and 8.2% for P102L-M129V. But, again, this percentage remains within the NMR-derived percentages of various PrPs: 3.8% for wild-type PrP and 8.7% for R220K [42]. Finally, the total number of native interactions with time is conserved upon mutation (fig. 1D). Taken together,

these results indicate that the mutations P102L and P102L-M129V likely have a small effect on the overall conformational properties of the protein core. This is consistent with the circular dichroism (CD) analysis of Swietnicki et al. [21] on human PrP90–231(P102L). The discrepancy with the work of Cappai et al. [20], which points to a significant decrease in α helix content in mouse PrP23–231(P101L), is not clear. It may be explained by the fact that the mutation may exert its effect on a much longer timescale or in the full-length PrP protein alone. Such a study is clearly beyond the scope of the present work. Comparison of the NMR spectra of PrP23–231 and PrP90–231 containing mutation P102L would help clarify these conflicting data.

In figure 1 C, we see that the tail is more mobile in P102L (run 2) and P102L-M129V than in wild-type PrP. Do these mutations induce the formation of a transient three-stranded antiparallel β sheet within the tail as was determined by MD simulations on the M129V and G131V variants [15]? Specifically, we found that the population of this β sheet spanning approximately residues 131–127 (S1 strand), 122–120 and 114–112 is ~30% for both variants and that the rate-limiting factor for β sheet formation in wild-type PrP90-231 is thermodynamic rather than kinetic in character. MD analysis of the P102L and P102L-M129V variants shows that the tail explores a β hairpin spanning residues 130–127 and 121–118 (70% of the simulation time) along with disordered states (30%) as determined for wild-type PrP. Thus, the replacement of the β sheet breaker amino acid at position 102 does not propagate the β sheet within the tail on the nanosecond timescale.

Deletion mutants have different effects on PrP stability

To determine the impact of the deletion of each strand on PrP, MD simulations were carried out at two distinct temperatures. For clarity in what follows, we keep the wild-type numbering of the amino acids in the deletion variants. Furthermore, the percentage of native contacts is evaluated by expressing the total number of contacts in a given structure over the total number of contacts in the native structure of wild-type PrP. This allows us to measure the stability of wild-type PrP contacts in the deletion variants.

The minimized structures of the PrP-S1 and PrP-S2 variants, shown in figure 2 A, B, deviate by 2.1 and 1.5 Å from that of wild-type PrP. The RMS deviation is located be-

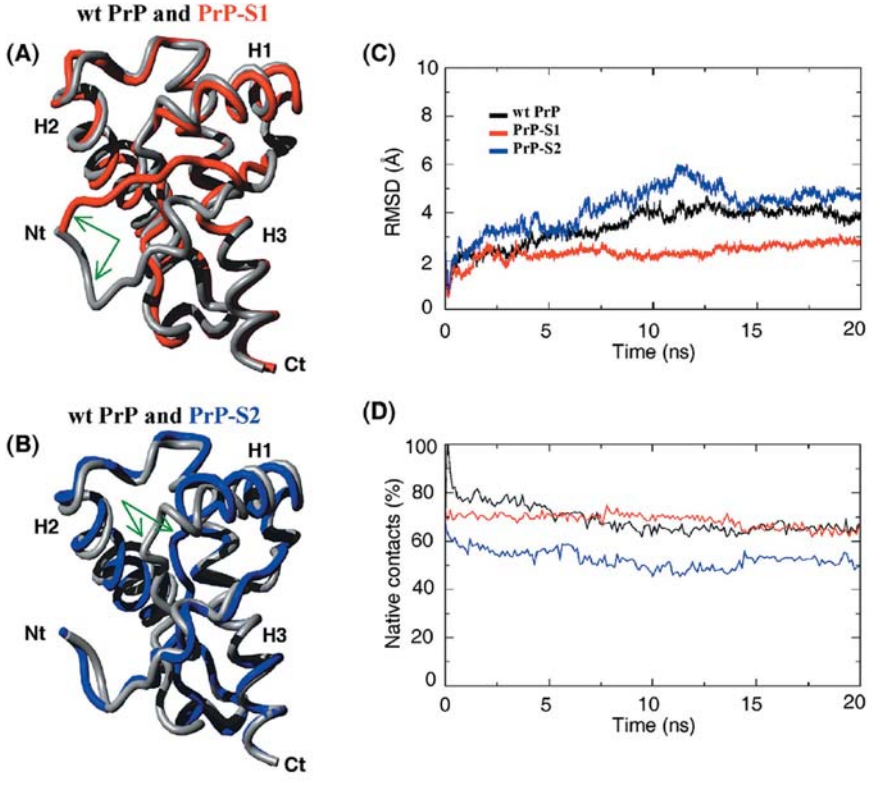

Figure 2. (*A, B*) Simulations of wild-type PrP and its PrP-S1 and PrP-S2 variants at 298 K. Superposition of the minimized PrP-S1 (*A*) (red) and PrP-S2 (*B*) (blue) structures on wild-type PrP (gray). For clarity, only residues 124–226 are shown. The structural changes upon strand deletion are indicated by arrows (see details in the text). (*C, D*) RMS deviations from the MD average NMR structure of the residues 128–214 as a function of time (*C*). Percentage of native wild-type PrP contacts as a function of time (*D*). Red, PrP-S1; blue, PrP-S2; black, wild-type PrP.

tween positions Gly124 and Met138 in PrP-S1 and between Asn153 and Val166 in PrP-S2. A comparison was first made of the secondary-structure composition generated at 320 K in order to estimate the relative stability of each helix and β strand. We found that the α helix content changes little upon S1 deletion (55% vs 51% in wild-type PrP), but drops to 42% in PrP-S2 because of the destabilization of helix H2 and the C-terminal end of helix H1 (table 1). The β strand content is 0% in PrP-S1 and 4.8% in PrP-S2 versus 3.9% in wild-type PrP. Analysis of the percentage of native contacts as a function of time shows that PrP-S1 and wild-type PrP behave similarly (~63% and 67%, respectively), but PrP-S2 is destabilized (~47%) on a 4-ns timescale (data not shown). These findings are supported by the 20-ns simulations at 298 K.

Analysis of the Cα RMS deviations generated at 298 K as a function of time in figure 2C shows that PrP-S1 deviates less from its starting structure than wild-type PrP during the 20-ns timescale (mean RMSD of 2.0 Å for PrP-S1 vs 3.5 Å for wild-type PrP) and that PrP-S2 is very flexible (mean RMSD of 4.5 Å). In this analysis, we used residues 128–214 because the C-terminal end of helix H3 is very flexible as determined by hydrogen exchange and NMR relaxation studies of human and Syrian hamster PrP [40]. Secondary-structure composition at 298 K shows that the mean percentage of α helix within the protein core varies upon strand deletion from 34% in PrP-S2 to 47% in PrP-S1 versus 57% in wild-type PrP by MD and NMR. Clearly, the predicted percentage of α helix in PrP-S2 is much shorter than that identified by NMR for various PrPs. For PrP-S1, the situation is less clear because the C-terminal end of helices H2 and H3 varies between species NMR: helix H2 is 12 residues shorter (173–182) in human PrP125–228(S170N) [42] – this leads to 48% of α helix versus 47% for PrP-S1 – and helix H3 spans residues 200–222 in mouse PrP121–231 [3] versus 200–228 in human PrP90–231 [5]. The mean percentage of β strand at 298 K is 0% in PrP-S1 and 1.1% in PrP-S2 versus 7.8% in wild-type PrP by MD and NMR. Thus, there is no β sheet in the S1-deleted variant, but a β hairpin forms in wild-type PrP and the S2-deleted variant from residues 120–122 and 128–130 (S1 strand) for 90% and 30% of the simulation time, respectively. The percentage of native contacts at 298 K with time, in figure 2D, is invariant upon deletion of strand S1, but is reduced upon deletion of strand S2. We see that the percentage of native contacts at 20 ns is 67% in PrP-S1 and 50% in PrP-S2 versus 67% in wild-type PrP. Taken together, the RMS deviation, the percentage of native contacts and the secondary structure analysis indicate that deletion of strand S2 changes the global (stability) three-dimensional PrP structure, while removal of strand S1 does not lead to major tertiary-structure variation within the core. This is consistent with the hypotheses of Vorberg et al. [26] based on the NMR structure of wild-type PrP.

Deletion mutants modify the binding and conversion sites targeted by PrP^{Sc}

Transition from PrP^{C} to PrP^{Sc} is a two-step process, which begins with binding between the two PrP isoforms, followed by conversion of the cellular to the pathogenic form [43]. In hamster PrP, the binding surfaces include residues 119–138, 165–174 and 206–223, while conversion to PrP^{Sc} is strongly influenced by residues 139, 155 and 170 [43].

Figure 3A–C shows for each PrP the conformation representing 84% (PrP-S1), 98% (PrP-S2) and 55% (wild-type PrP) of the MD-generated structures from 15 to 20 ns, using cluster analysis and an RMSD cut-off of 2 Å for residues 90–231. In both deletion variants, the three binding regions spanning helix H3 (206–223), the loop between S2 and H2 (165–175) and the N-terminal sequence (119–138) move substantially from their positions in the NMR structure of wild-type PrP. The C-terminal end of helix H3 (215–223) is disordered in both variants and can even interact with the tail in PrP-S1 (residues M213 and Q217 are in contact with residue A118). The binding site 165–175 is much more dynamic and the conformation of the N-terminal tail is substantially modified. The residues (G119, M138) move by (11 Å, 8 Å) and (22 Å, 6 Å) from the NMR wild-type PrP structure to the representative PrP-S1 and PrP-S2 forms, respectively. Moreover, deletion of strand S2 does not prevent the formation of a β sheet spanning S1 (130–128) and the tail (122–120), while deletion of strand S1 blocks or (may delay) the formation of a β sheet within the tail.

Along with a change in the shape of the three binding sites, removal of the β strands also changes the position (see fig. 3) and solvent accessibility of the residues important for conversion. Met139 becomes totally buried in PrP-S1 [its solvent accessibility surface (SAS) is 4 $Å^2$ vs 46 $Å^2$ in the NMR structure) and the residues Asn155 and Asn170 are less exposed to solvent. Their SASs are (100 $Å^2$, 111 $Å^2$) in PrP-S1 and (94 $Å^2$, 71 $Å^2$) in PrP-S2 versus (130 $Å^2$, 122 $Å^2$) in the wild-type PrP structure.

Helix 1 is rather stable and helices 2 and 3 are disordered in deletion mutants

The MD-generated structures of wild-type PrP during the 20-ns timescale can be clustered into two conformations: one (55%) with helix H1 spanning residues 144–153, H2 residues 172–194 and H3 residues 200–226, in perfect agreement with the NMR positions; the other (45%) with H1 residues 144–156, H2 residues 172–194 and H3 residues 200–226. In the representative MD form of the variants, we find that the α helix content of the fragment spanning helix H3 is reduced by 44%. The N-terminal end of helix H3 remains formed (residues 200–214) and the fragment 215–226 unfolds in PrP-S2, while H3 spans residues 200–209 and 212–216 in PrP-S1. These find-

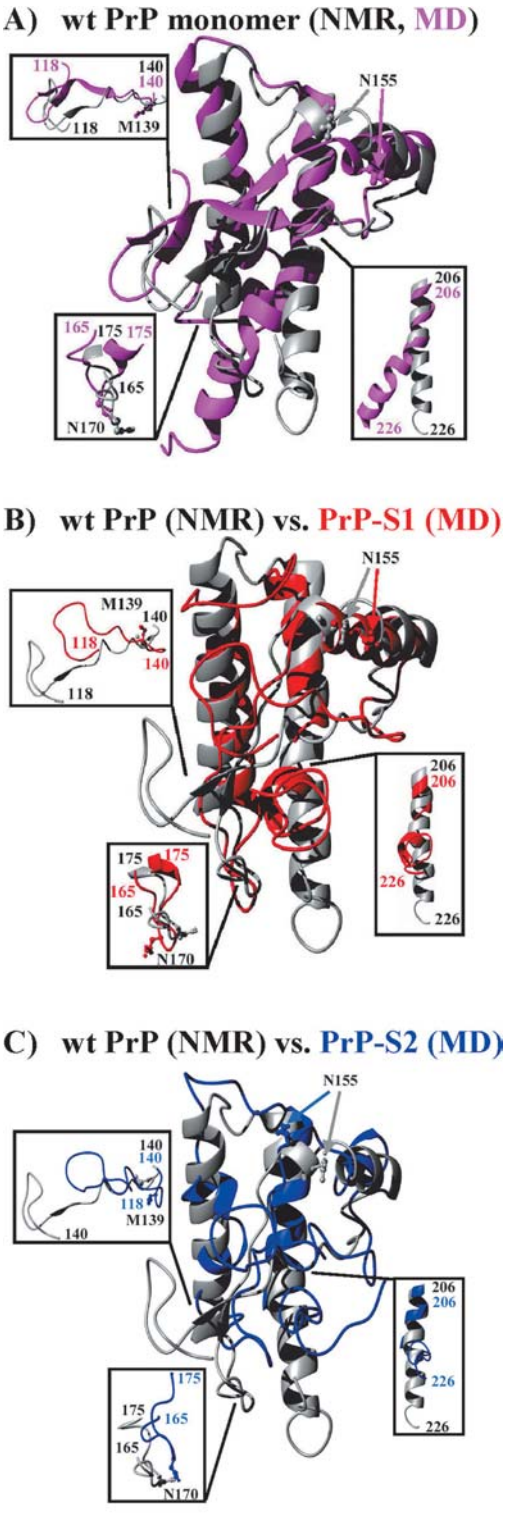

Figure 3. Superposition of the NMR structure of wild-type PrP (gray) on the most populated conformation of wild-type PrP (*A*) (magenta), PrP-S1 (*B*) (red) and PrP-S2 (*C*) (blue) from 15 to 20 ns (see text). The N and C terminals correspond to residues 118 and 231, respectively. For clarity, the three regions involved in binding of the two isoforms, namely spanning residues 119–138, 165–175 (between strand S2 and helix H2) and 206–223 (helix H3) [43], are also shown in boxes. The residues Met139, Asn155 and Asn170, important for conversion, are represented at an atomistic detail [43].

ings are in line with a number of studies. These include hydrogen exchange and NMR relaxation of PrPs in their normal structures [40], sequence analysis which proposes that residues 204–216 stay invariant through conversion [8, 44], and the discovery of the antibody V5B2, raised against residues 214–226, which recognizes PrP^{Sc} but not PrP^{C}, indicating a structural rearrangement of the C terminus [45].

The α helix content of H2 is reduced by 36% upon S1 deletion and 64% upon S2 deletion. H2 spans residues 173–188 in PrP-S1, while H2 spans residues 179–183 and 185–188 in PrP-S2 versus residues 172–194 by MD and NMR. This high propensity to unfold in both variants correlates well with recent studies which identified helix H2 as frustrated in its monomeric PrP^{C} structure [46, 47]. Frustration in secondary structure elements is defined as the incompatibility between the predicted (by using neural networks, for example) secondary structure and the experimentally determined structure. This is also in agreement with biophysical studies on the fragment spanning helices H2 and H3 which showed that the full tertiary structure context of PrP is critical to stabilize the C-terminal α-helical hairpin [25]. We emphasize that the disorder of helices H2 and H3 may be reduced in PrP-S1 and PrP-S2 spanning residues 23–231 because of transient interactions between the N-terminal octarepeat region and the protein core [2, 41]. But such a disorder occurs because it is an intrinsic property of PrP: helices H2 and H3 span residues 171–188 and 200–223 in the crystal structure of human PrP119–226 [5] versus residues 173–182 and 200–227 in the NMR structure of human PrP125–228(S170N) [42].

In contrast to helices H2 and H3 which are disordered upon β strand deletion, helix H1 is found to be rather stable. Helix H1 is fully formed upon removal of strand S1. Helix H1 spans residues 145–149 upon removal of strand S2 because of favorable interactions between Tyr145 and Tyr149, and between Asp144, Glu146, Asp147 and the dipole moment of the helix. This finding is fully consistent with CD and NMR studies of human and murine prion peptides encompassing helix 1 and flanking sequences under various pH conditions [48, 49]. Moreover, helix H1 was recently found to have the highest thermodynamic stability among the three helices [50], and helix H1 is the most stable secondary-structure element at low pH by MD simulations of human PrP(125–228) [51]. Taken together, these data exclude the possibility that the high stability of H1 as discussed here results from a smaller chance of being hit by random effects because H1 is much shorter than H2 and H3.

Conclusions

The formation of PrP^{Sc} involves a decrease in α helix content and a substantial increase in β strand content [6]. Within the 'protein-only' hypothesis, a detailed mecha-

nism for this conversion of secondary structure is unclear, but both the tail and the core are implicated in the conformational transition [52]. We investigated the impact of the point mutation P102L and the deletion of either the first or the second β strand on PrP(90–231) structure and dynamics. By using PrP mutants in isolation, we do not expect that their MD-generated forms are similar to the scrapie form. These PrP mutants can, however, provide insights into the early steps in PrP interconversion, as reported for amyloidogenic mutants of proteins such as lysozyme [53] and transthyretin [54].

Figure 4 summarizes the likely biologically important fluctuations of the secondary structures of PrP as determined by our MD predictions. MD analysis of wild-type PrP and its variants shows that the point mutations M129V and G131V extend the short β sheet in the normal protein into a larger sheet at neutral pH, but P102L does not (see fig. 4). This result is significant because it shows that all pathogenic mutations do not exert a uniform effect in promoting β sheet conformation, which is further stabilized by interactions with PrP^{Sc}.

Based on a total of 60-ns MD trajectories at room temperature, PrP-S1 is found to fluctuate around the native structure of wild-type PrP, while PrP-S2 explores partially unfolded conformations. Since the topological conversion is not abolished in a cell-free assay system, the PrP-S1 and PrP-S2 forms retain some of the structural features recognized by PrP^{Sc}. In both variants, the N-terminal tail and all residues involved in binding and conversion are, however, subjected to significant conformational changes. This finding confirms that partially unfolded intermediates of molten globule type are involved in the structural transition [50, 55]. Intriguing in this context is that our PrP-S2 structure with disordered helices H2 and H3 but well-formed helix H1 resembles the conformation of Syrian hamster PrP90–231 determined by high-pressure NMR experiments and identified as a PrP intermediate or a closely related precursor [50]. There is, however, no available detailed experimental structure for exact comparison.

Finally, our MD simulations indicate that helix H1 spanning residues 144–153 in the NMR structure of wild-type PrP, and lacking point mutations associated with known human prion diseases, is rather stable against environmental perturbations (fig. 4). This finding, which complements spectroscopic studies of prion peptides lacking the full tertiary context of PrP [48, 49], demonstrates that unfolding of the full domain containing helix H1 is not an early step in PrP interconversion. In addition, figure 4 offers no really compelling evidence that helices H2 and H3 are more stable than H1 and that they are able to survive the transformation to the scrapie form while helix H1 is not. This result raises the question whether the N-terminal end of helix H1 may retain its structure in PrP^{Sc}. Recently, the model of Wille et al. [7] with α helices H2 and H3 formed and β helices in the region 90–170 has been questioned using sequence analysis [8, 44] and vibrational Raman optical activity [56]. The presence of partial helix H1 in PrP^{Sc} is also compatible with the in vivo inhibitory effects on prion replication using the monoclonal antibody ICSM18 recognizing residues 146–159 of murine PrP^{C} and having a lower affinity for

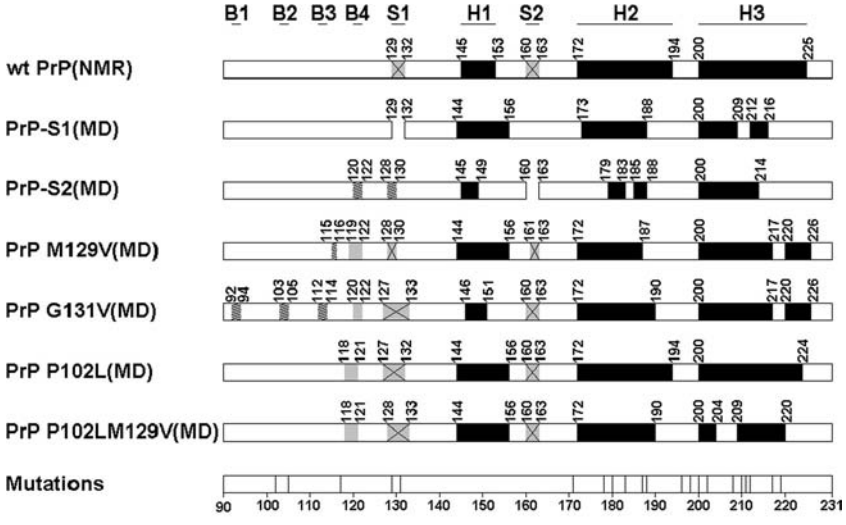

Figure 4. Schematic representation of the secondary structures of wild-type recombinant Syrian hamster PrP90-231 by NMR [2] and its variants from the present (PrP-S1, PrP-S2, P102L and P102L-M129V) and previous (M129V and G131V [15]) MD simulations. H1, H2 and H3 are presented by black boxes; S1 and S2 by gray boxes with crosses; permanent β strands within the tail by gray boxes and transient β strands within the tail (formed less than 50% of the simulation time) by cross-hatched boxes. B1, B2, B3 and B4 are β-strands within the tail. Deletion of S1 and S2 strands is shown as a gap. Point mutations associated with known human prion diseases are: P102L, P105L, A117V, G131V, D178N, V180I, T183A, H187R, T188R, E196K, F198S, E200K, D202N, R208H, V210I, E211Q, Q212P and Q217R; polymorphism: M129V, E219K; unclassified: N171S as found in SWISS-PROT entry P04156 [59].

PrP^{Sc} [57]. Moreover, the monoclonal antibody 15B3, which recognizes PrP^{Sc} at positions 142–148 (N-terminal half of helix H1 in the normal protein), 162–170 and 214–226, does not necessarily require a structural rearrangement of the full helix H1 [8, 58].

Acknowledgements. S. Santini is supported by the Natural Sciences and Engineering Research Council of Canada. The calculations were done on the computers at IGS in Marseille. We thank Dr Melki and Dr Cappai for helpful discussions.

1 Prusiner S. B. (1998) Prions. Proc. Natl. Acad. Sci. USA **95:** 13363–13383
2 Donne D. G., Viles J. H., Groth D., Mehlhorn I., James T. L., Cohen F. E. et al. (1997) Structure of the recombinant full-length hamster prion protein PrP(29–231): the N terminus is highly flexible. Proc. Natl. Acad. Sci. USA **94:** 13452–13457
3 Riek R., Hornemann S., Wider G., Billeter M., Glockshuber R. and Wüthrich K. (1996) NMR structure of the mouse prion protein domain PrP(121-321). Nature **382:** 180–182
4 Knaus K. J., Morillas M., Swietnicki W., Malone M., Surewicz W. K. and Yee V .C. (2001) Crystal structure of the human prion protein reveals a mechanism for oligomerization. Nat. Struct. Biol. **8:** 770–774
5 Zahn R., Liu A., Luhrs T., Riek R., Schroetter C. von, Lopez Garcia F. et al. (2000). NMR solution structure of the human prion protein. Proc. Natl. Acad. Sci. USA **97:** 145–150
6 Caughey B. W., Dong A., Bhat K., Ernst D., Hayes S. and Caughey W. (1991) Secondary structure analysis of the scrapie-associated protein PrP 27–30 in water by infrared spectroscopy. Biochemistry **30:** 7672–7680
7 Wille H., Michelitsch M. D., Guenebaut V., Supattapone S., Serban A., Cohen F. E. et al. (2002) Structural studies of the scrapie prion protein by electron crystallography. Proc. Natl. Acad. Sci. USA **99:** 3563–3568
8 Mornon J. P., Prat K., Dupuis F., Boisset N. and Callebaut I. (2002) Structural features of prions explored by sequence analysis. II. A PrP(Sc) model. Cell. Mol. Life Sci. **59:** 2144–2154
9 Jackson G. S. and Collinge J. (2001) The molecular pathology of CJD: old and new variants. J. Clin. Pathol. Mol. Pathol. **54:** 393–399
10 Panegyres P. K., Toufexis K., Kakulas B. A., Cernevakova L., Brown P., Ghetti B. et al. (2001) A new PRNP mutation (G131V) associated with Gerstmann-Straussler-Scheinker disease. Arch. Neurol. **58:** 1899–1902
11 Cohen F. E., Pan K., Huang Z., Baldwin M., Fletterick R. and Prusiner S. B. (1994) Structural clues to prion replication. Science **264:** 530–531
12 Liemann S. and Glockshuber R. (1999) Influence of amino acid substitutions related to inherited human prion diseases on the thermodynamic stability of the cellular prion protein. Biochemistry **38:** 3258–3267
13 Vanik D. L. and Surewicz W. K. (2002) Disease-associated F198S mutation increases the propensity of the recombinant prion protein for conformational conversion to scrapie-like form. J. Biol. Chem. **277:** 49065–49070
14 Zhang Y., Swietnicki W., Zagorski M. G., Surewicz W. K. and Sonnichsen F. D. (2000) Solution structure of the E200K variant of human prion protein. J. Biol. Chem. **275:** 33650–33654
15 Santini S., Claude J. B., Audic S. and Derreumaux P. (2003) Impact of the tail and mutations G131V and M129V on prion protein flexibility. Proteins **51:** 258–265
16 Okimoto N., Yamanaka K., Suenaga A., Hata M. and Hoshino T. (2002) Computational studies on prion proteins: effect of ala(117)-val mutation. Biophys. J. **82:** 2746–2757
17 Gsponer J., Ferrara P. and Caflisch A. (2001) Flexibility of the murine prion protein and its Asp178Asn mutant investigated by molecular dynamics simulations. J. Mol. Graph. Model. **20:** 169–182
18 Billeter M., and Wüthrich K. (2000) The prion protein globular domain and disease-related mutants studied by molecular dynamics simulations. Arch. Virol. Suppl. **16:** 251–63
19 Barron R. M., Thomson V., Jamieson E., Melton D. W., Ironside J., Will R. et al. (2001) Changing a single amino acid in the N-terminus of murine PrP alters TSE incubation time across three species barriers. EMBO J. **20:** 5070–5078
20 Cappai R., Stewart L., Jobling M., Thyer J., White A., Beyreuther K. et al. (1999) Familial prion disease mutation alters the secondary structure of recombinant mouse prion protein: implications for the mechanism of prion formation. Biochemistry **38:** 3280–3284
21 Swietnicki W., Petersen R., Gambetti P. and Surewicz W. (1998) Familial mutations and the thermodynamic stability of the recombinant human prion protein. J. Biol. Chem. **273:** 31048–31052
22 Young K., Jones C. K., Piccardo P., Lazzarini A., Golbe L. I., Zimmerman T. R. Jr. et al. (1995) Gerstmann-Straussler-Scheinker disease with mutation at codon 102 and methionine at codon 129 of PRNP in previously unreported patients. Neurology **45:** 1127–1134
23 Soto C., Kascsak R. J., Saborio G. P., Aucouturier P., Wisniewski T., Prelli F. et al. (2000) Reversion of prion protein conformational changes by synthetic β-sheet breaker peptides. Lancet **355:** 192–197
24 Caughey B., Raymond L. D., Raymond G. J., Maxson L., Silveira J., and Baron G. S. (2003) Inhibition of protease-resistant prion protein accumulation in vitro by curcumin. J. Virol. **77:** 5499–5502
25 Eberl H. and Glockshuber R. (2002) Folding and intrinsic stability of deletion variants of PrP(121–231), the folded C-terminal domain of the prion protein. Biophys. Chem. **96:** 293–303
26 Vorberg I., Chan K. and Priola A. (2001) Deletion of β-strand and α-helix secondary structure in normal prion protein inhibits formation of its protease-resistant isoform. J. Virol. **75:** 10024–10032
27 Berendsen H. J. C., Spoel D. van der and Drunen R. van (1995) GROMACS: A message-passing parallel molecular dynamics implementation. Comp. Phys. Commun. **91:** 43–56
28 James T. L., Liu H., Ulyanov N. B., Farr-Jones S., Zhang H., Donne D. G. et al. (1997) Solution structure of a 142-residue recombinant prion protein corresponding to the infectious fragment of the scrapie isoform. Proc. Natl. Acad. Sci. USA **94:** 10086–10091
29 Guex N. and Peitsch M. C. (1997) SWISS-MODEL and the Swiss-PdbViewer: an environment for comparative protein modelling. Electrophoresis **18:** 2714–2723
30 Lazaridis T. and Karplus M. (1998) Discrimination of the native from misfolded protein models with an energy function including implicit solvation. J. Mol. Biol. **288:** 477–487
31 Alonso D. O., DeArmond S. J., Cohen F. E. and Daggett V. (2001) Mapping the early steps in the pH-induced conformational conversion of the prion protein. Proc. Natl. Acad. Sci. USA **98:** 2985–2989
32 Rezaei H., Marc D., Choiset Y., Takahashi M., Hui Bon Hoa G., Haertle T. et al. (2000) High yield purification and physico chemical properties of full length recombinant allelic variants of sheep prion protein linked to scrapie susceptibility. Eur. J. Biochem. **267:** 2833–2839
33 Kabsch W. and Sander C. (1983) Dictionary of protein secondary structure: pattern recognition of hydrogen-bonded and geometrical features. Biopolymers **22:** 2577–2637
34 Day R., Bennion B. J., Ham S. and Daggett V. (2002) Increasing temperature accelerates protein unfolding without changing the pathway of unfolding. J. Mol. Biol. **322:** 189–203

35 Fraczkiewicz R. and Braun W. (1998) Exact and efficient analytical calculation of the accessible surface area and their gradient for macromolecules. J. Comp. Chem. **19:** 319–333
36 Koradi R., Billeter M. and Wüthrich K. (1996) MOLMOL: a program for display and analysis of macromolecular structures. J. Mol. Graph. **14:** 51
37 Alonso D. O., An C. and Daggett V. (2002) Simulations of biomolecules: characterization of the early steps in the pH-induced conformational conversion of the hamster, bovine and human forms of the prion protein. Phil. Trans. A Math. Phys. Eng. Sci. **360:** 1165–1178
38 Wildegger G., Liemann S. and Glockshuber R. (1999) Extremely rapid folding of the C-terminal domain of the prion protein without kinetic intermediates. Nat. Struct. Biol. **6:** 550–553
39 Duan Y. and Kollman P. (1998) Pathways to a protein folding intermediate observed in a 1-microsecond simulation in aqueous solution. Science **282:** 740–744
40 Hosszu L. L., Baxter N. J., Jackson G. S., Power A., Clarke A. R., Waltho J. P. et al. (1999) Structural mobility of the human prion protein probed by backbone hydrogen exchange. Nat. Struct. Biol. **6:** 740–743
41 Viles J. H., Donne D., Kroon G., Prusiner S. B., Cohen F. E., Dyson H. J. et al. (2001) Local structural plasticity of the prion protein: analysis of NMR relaxation dynamics. Biochemistry **40:** 2743–2753
42 Calzolai L., Lysek D. A., Guntert P., Schroetter C. von, Riek R., Zahn R. et al. (2000) NMR structures of three single-residue variants of the human prion protein. Proc. Natl. Acad. Sci. USA **97:** 8340–8345
43 Horiuchi M., Priola S. A., Cabry J. and Caughey B. (2000) Interactions between heterologous forms of prion protein: binding, inhibition of conversion, and species barriers. Proc. Natl. Acad. Sci. USA **97:** 5836–5841
44 Mornon J. P., Prat K., Dupuis F. and Callebaut I. (2002) Structural features of prions explored by sequence analysis. I. Sequence data. Cell. Mol. Life Sci. **59:** 1366–1376
45 Serbec C. V., Bresjanac M., Popovic M., Hartman P. K., Galvani V., Rupreht R. et al. (in press) Monoclonal antibody against a peptide of human prion protein discriminates between Creutzfeldt-Jacob's disease-affected and normal brain tissue. J. Biol. Chem.
46 Kallberg Y., Gustafsson M., Persson B., Thyberg J. and Johansson J. (2001) Prediction of amyloid fibril-forming proteins. J. Biol. Chem. **276:** 12945–12950
47 Dima R. I. and Thirumalai D. (2002) Exploring the propensities of helices in PrP(C) to form beta sheet using NMR structures and sequence alignments. Biophys. J. **83:** 1268–1280
48 Ziegler J., Sticht H., Marx U. C., Muller W., Rosch P. and Schwarzinger S. (2003) CD- and NMR-studies of prion protein helix 1: novel implications for its role in the PrPC PrPSc conversion process. J. Biol. Chem. **278:** 50175–50181
49 Jamin N., Coic Y. M., Landon C., Ovtracht L., Baleux F., Neumann J. M. et al. (2002) Most of the structural elements of the globular domain of murine prion protein form fibrils with predominant beta-sheet structure. FEBS Lett. **529:** 256–260
50 Kuwata K., Li H., Yamada H., Legname G., Prusiner S. B., Akasaka K. et al. (2002) Locally disordered conformer of the hamster prion protein: a crucial intermediate to PrPSc? Biochemistry **41:** 12277–12283
51 Gu W., Wang T., Zhu J., Shi Y. and Liu H. (2003) Molecular dynamics simulation of the unfolding of the human prion protein domain under low pH and high temperature conditions. Biophys. Chem. **104:** 79–94
52 Hornemann S. and Glockshuber R. (1998) A scrapie-like unfolding intermediate of the prion protein domain PrP (121–231) induced by acidic pH. Proc. Natl. Acad. Sci. USA **95:** 6010– 6014
53 Moraitakis G. and Goodfellow J. M. (2003) Simulations of human lysozyme: probing the conformations triggering amyloidosis. Biophys. J. **84:** 2149–2158
54 Yang M., Lei M. and Huo S. (2003) Why is Leu55 → Pro55 transthyretin variant the most amyloidogenic: insights from molecular dynamics simulations of transthyretin monomers. Protein Sci. **12:** 1222–1231
55 Apetri A. C, and Surewicz W. K. (2002) Kinetic intermediate in the folding of human prion protein. J. Biol. Chem. **277:** 44589–44592
56 McColl I. H., Blanch E. W., Gill A. C., Rhie A. G., Ritchie M. A., Hecht L. et al. (2003) A new perspective on beta-sheet structures using vibrational Raman optical activity: from poly(L-lysine) to the prion protein. J. Am. Chem. Soc. **125:** 10019–10026
57 White A. R., Enever P., Tayebi M., Mushens R., Linehan J., Brandner S. et al. (2003) Monoclonal antibodies inhibit prion replication and delay the development of prion disease. Nature **422:** 80–83
58 Korth C., Stierli B., Streit P., Moser M., Schaller O., Fischer R. et al. (1997) Prion (PrPSc)-specific epitope defined by a monoclonal antibody. Nature **390:** 74–77
59 Boeckmann B., Bairoch A., Apweiler R., Blatter M.-C., Estreicher A., Gasteiger E. et al. (2003) The SWISS-PROT protein knowledgebase and its supplement TrEMBL in 2003. Nucleic Acids Res. **31:** 365–370